Generalized eigenproblem method for surface and interface states: The complex bands of GaAs and AlAs

Timothy B. Boykin*
Department of Electrical and Computer Engineering, The University of Alabama in Huntsville, Huntsville, Alabama 35899
(Received 1 February 1996; revised manuscript received 2 April 1996)

A proper calculation of the complex band structure is essential for accurately obtaining the energy levels of quantum wells, or the resonances of resonant tunneling diodes. Most present empirical tight-binding calculations are based upon the nearest-neighbor sp^3s^* model, and determine the complex band structure via a transfer-matrix-type equation. This procedure will fail at certain values of the in-plane wave vector $\mathbf{k}_\parallel$ or for certain parameter sets; other methods are unsuitable since they do not fully address this problem. Additionally, the nearest-neighbor sp^3s^* model typically does a rather poor job reproducing the X-valley transverse effective mass. More complete calculations thus require an improved method for finding the complex bands and a more complete underlying tight-binding model. Here we develop a method which easily handles those $\mathbf{k}_\parallel$ at, or parameter sets for, which other approaches fail and implement it in the second-near neighbor sp^3s^* model to find the complex bands of GaAs and AlAs. We also give the change of basis necessary to transform the equations into a real system, thus allowing for a more efficient calculation. [S0163-1829(96)03535-7]

I. INTRODUCTION

Complex band structures of semiconductor materials are of interest for a variety of reasons. In the first place, complex bands give the surface states of the bulk semiconductor. Of greater import is their use in determining the energy levels of heterostructures such as quantum wells, and the resonances of resonant tunneling diodes as calculated with models more complete than the effective-mass approach (e.g., empirical tight-binding models). Specifically, in the latter context, eigenvectors corresponding to the various complex bands serve as the basis in terms of which the total state is expanded in some region; that is, they are used in formulating the boundary conditions. Consider a planar structure such as a quantum well, where the state is expanded in some layer. Here the bulk crystal periodicity is lost in one direction so that one expresses the eigenvectors in the planar-orbital basis, where the Bloch sums are eigenstates of the in-plane wave vector $\mathbf{k}_\parallel$. (For an [001]-oriented device the layers of the constituent materials lie perpendicular to the z axis, and $\mathbf{k}_\parallel = k_x\mathbf{e}_x + k_y\mathbf{e}_y$.) On first inspection, determination of the complex band structure appears to present no great challenges: one simply chooses an underlying tight-binding model, such as the nearest-neighbor sp^3s^* model of Vogl, Hjalmarson, and Dow,[1] and finds the eigenvectors and complex-k_z eigenvalues using the transfer-matrix method.[2] While the simplicity of this procedure is well known and has doubtless led to its wide adoption (it is employed in the majority of empirical tight-binding calculations for aperiodic heterostructures), what is *not* generally recognized is that there are circumstances in which it will fail.

This difficulty is most immediately recognizable when one attempts to apply the foregoing procedure to the case of indirect semiconductors, for example, those in which the X valleys are of greatest interest. In the first place, the nearest-neighbor sp^3s^* model[1] produces an exceedingly poor fit to the X-valley transverse effective mass for most materials; indeed, it is incapable of fitting the transverse-X mass at the X point.[3] More troublesome than even this is the transfer-matrix method[2] itself. Because it requires matrix inversions, it may not be usable with certain parameter sets or at certain $\mathbf{k}_\parallel$ (e.g., $\mathbf{k}_\parallel = 2\pi/a\,\mathbf{e}_x$, where a is the lattice constant): in these circumstances the transfer matrix *does not exist*. We emphasize that the nonexistence of a transfer matrix is not unique to the nearest-neighbor sp^3s^* model: in [001]-oriented zinc-blende crystals the transfer matrix does not exist at this $\mathbf{k}_\parallel$ even in the second-near-neighbor sp^3 and sp^3s^* models, which *can* correctly reproduce the X-valley transverse mass. For indirect semiconductors, then, the failure of this commonly used procedure is quite serious, for one *cannot* determine the complex band structure in the most important region of $\mathbf{k}_\parallel$ space. Note, too, that this observation applies even to fully coherent calculations. Furthermore, calculations incorporating inelastic processes, since they mix levels of different $\mathbf{k}_\parallel$, will experience similar problems; this is especially true of calculations for structures incorporating indirect semiconductor layers. Hence we require another procedure: one which is based upon an underlying bulk band structure model providing a good approximation for all gaps and effective masses in the energy range of interest, and which has a complex band-structure calculation method applicable for *all* $\mathbf{k}_\parallel$.

The first requirement clearly calls for a more complete model. We note that second-near-neighbor sp^3 models can be parametrized to give a good fit of the X-valley transverse mass, but still do not well approximate light Γ-valley conduction-band masses; the parameters of Talwar and Ting,[4] although generally superior to others, are still insufficient. A third-near-neighbor model similar to that of Tserbak, Polatoglu, and Theodorou[5] is certainly an option; however, its longer-range interactions make calculations for

planar structures like quantum wells more computationally intensive. Instead, we note the improved conduction-band fit afforded by the nearest-neighbor sp^3s^* model over the nearest-neighbor sp^3 model,[1] and accordingly employ an sp^3s^* model having interactions up to second-near neighbor as well as spin-orbit coupling.

The second requirement poses a greater challenge, for no currently available complex band-structure calculation method satisfies it. Consider first the method of Chang:[6] although it does not assume the invertibility of the coupling matrices which can become singular, it has numerical difficulties for characteristic polynomials of large order,[7] and, as we shall see below, in the case of singular coupling matrices it will not find all of the eigenvalues. These difficulties, along with our introduction of a large underlying band-structure model, render it unsuitable. We next consider the method of Chang and Schulman,[7] in which one partially reformulates the problem when certain coupling matrices become singular. Using this method one can calculate the complex bands in cases such as that of the nearest-neighbor sp^3s^* model[1] for an [001]-oriented zinc-blende crystal, in which the Hamiltonian couples to a given monolayer (two atomic planes) only one atomic plane from each of the nearest-neighbor monolayers. Bowen *et al.*[8] give a related approach for dealing with this problem, specifically discussing the case of the nearest-neighbor sp^3s^* model.[1] Nevertheless, as valuable as these methods are, neither one addresses the invertibility issue at special $\mathbf{k}_\parallel$ (hereafter denoted singular points). Indeed, this problem of invertibility at certain $\mathbf{k}_\parallel$ is of a rather different nature from the limited range of coupling problem, for far away from the singular points the coupling matrices are quite well behaved and are easily and accurately inverted. As $\mathbf{k}_\parallel$ approaches one of the singular points, the matrices gradually become more nearly singular, and, since these calculations are usually performed numerically, with finite-precision arithmetic, the quality of the computed inverses becomes progressively worse. Dealing with this problem therefore requires an approach valid for *all* $\mathbf{k}_\parallel$. Hence we must find another method for calculating the complex band structure.

In this paper we calculate the complex bands of GaAs and AlAs for the [001] face using the second-near-neighbor sp^3s^* model, carrying out the computation as a generalized eigenproblem. We study the properties of this method, demonstrating that even in the case of singular coupling matrices the eigenvalues still have the required properties. Furthermore, in the process of demonstrating that the complex eigenvalues of this system come in conjugate pairs, we obtain the transformations necessary to turn the nominally complex problem into a real one *without* an increase in matrix dimension, which may be exploited to increase computational efficiency. Finally, we find that this method produces the correct complex bands even at those $\mathbf{k}_\parallel$ for which the transfer matrix does not exist (case of singular coupling matrices).

TABLE I. Tight-binding parameters (in eV) for GaAs and AlAs in the notation of Ref. 9; only nonzero parameters are listed. The AlAs same-site diagonal parameters have been adjusted to reflect the measured GaAs-AlAs conduction-band offset.

Parameter	GaAs	AlAs
$E_{sa,sa}^{(000)}$	−8.487 06	−8.203 43
$E_{pa,pa}^{(000)}$	0.387 69	−0.341 76
$E_{s^*a,s^*a}^{(000)}$	8.487 69	6.512 48
$E_{sc,sc}^{(000)}$	−2.861 11	−2.480 93
$E_{pc,pc}^{(000)}$	3.567 69	2.119 99
$E_{s^*c,s^*c}^{(000)}$	6.617 69	5.035 93
$4E_{sa,sc}^{(\frac{1}{2}\frac{1}{2}\frac{1}{2})}$	−6.544 53	−7.160 00
$4E_{sa,pc}^{(111/222)}$	4.680 00	5.072 00
$4E_{s^*a,pc}^{(111/222)}$	4.650 00	3.280 00
$4E_{pa,sc}^{(111/222)}$	8.000 00	7.500 00
$4E_{pa,s^*c}^{(111/222)}$	6.000 00	1.750 00
$4E_{x,x}^{(111/222)}$	2.136 95	1.940 00
$4E_{x,y}^{(\frac{1}{2}\frac{1}{2}\frac{1}{2})}$	5.170 00	4.850 00
$4E_{sa,sa}^{(110)}$	−0.010 00	−0.010 00
$4E_{sa,xa}^{(110)}$	0.050 00	0.040 00
$4E_{sa,xa}^{(011)}$	0.058 00	0.040 00
$4E_{s^*a,xa}^{(110)}$	0.020 00	0.020 00
$4E_{s^*a,xa}^{(011)}$	0.040 00	0.100 00
$4E_{xa,xa}^{(110)}$	0.320 00	0.602 20
$4E_{xa,xa}^{(011)}$	−0.050 00	−0.620 60
$4E_{xa,ya}^{(110)}$	1.240 00	0.660 00
$4E_{xa,ya}^{(011)}$	−1.000 00	−1.200 00
$4E_{sc,sc}^{(110)}$	−0.020 00	−0.010 00
$4E_{sc,xc}^{(110)}$	0.072 00	0.073 00
$4E_{sc,xc}^{(011)}$	0.020 00	0.040 00
$4E_{s^*c,xc}^{(110)}$	0.010 00	0.030 00
$4E_{s^*c,xc}^{(011)}$	0.093 50	0.030 00
$4E_{xc,xc}^{(110)}$	0.280 00	0.495 35
$4E_{xc,xc}^{(011)}$	−0.100 00	−0.166 95
$4E_{xc,yc}^{(110)}$	0.600 00	0.870 00
$4E_{xc,yc}^{(011)}$	−1.300 00	−1.700 00
λ_a	0.140 00	0.140 00
λ_c	0.058 00	0.008 00

II. METHOD

A. Derivation of the eigenproblem

The tight-binding parameters with which we describe GaAs and AlAs in the second-near-neighbor sp^3s^* model, using the notation of Slater and Koster,[9] appear in Table I. In our calculations we place the anions on the Bravais lattice sites, with the cations displaced by $\mathbf{v}=(a/4)(\mathbf{e}_x+\mathbf{e}_y+\mathbf{e}_z)$, where a is the conventional unit cell cube edge. Since the bulk Hamiltonian in the second-near-neighbor sp^3 model is given elsewhere,[4,10] and, owing to the identical symmetries of the s and s^* orbitals, the sp^3s^* second-near-neighbor Hamiltonian is easily derived from the former, we do not present the latter Hamiltonian. Instead we focus on interface systems, those having a disruption in translational symmetry along the z direction only.

In our calculation of the complex bands for the [001]-oriented face of GaAs and AlAs, we work in the planar orbital basis; in what follows the subscript $\parallel$ denotes a vector lying entirely in the $x-y$ plane (e.g., $\mathbf{k}_\parallel=k_x\mathbf{e}_x+k_y\mathbf{e}_y$). A layer is taken to be a plane of anions and the plane of cations

located $+(a/4)\mathbf{e}_z$ away, so that a layer occupies a space of $a/2$ along the z direction, while a sublayer is a plane of either anions or cations. The near-neighbor interactions then lead to couplings of adjacent sublayers, while the second-near-neighbor interactions result in both intralayer and adjacent layer couplings; the spin-orbit interaction gives rise to same-site couplings only. In this system, in the absence of other interactions or crystal imperfections, $\mathbf{k}_\parallel$ is a conserved quantity, as is the energy E. Thus the planar orbital basis states may be expressed in terms of the localized, orthogonal, atomiclike orbitals as

$$|n\mu\sigma;L;\mathbf{k}_\parallel\rangle=\frac{1}{\sqrt{N_\parallel}}\sum_{j=1}^{N_\parallel}\exp\{i\mathbf{k}_\parallel\cdot[\mathbf{R}_{j\parallel}(L)+\delta_{\mu,c}\mathbf{v}_\parallel]\}|n\mu\sigma;L;\mathbf{R}_{j\parallel}(L)+\delta_{\mu,c}\mathbf{v}_\parallel\rangle. \quad (1)$$

In (1), $N_\parallel$ is the number of atoms in the plane, n is the orbital type (one of s, x, y, z, or s^*), L indexes the layers, the atom type μ is either a (anion) or c (cation), the atom is located in the plane at $\mathbf{R}_{j\parallel}(L)+\delta_{\mu,c}\mathbf{v}_\parallel$, and $\sigma\in\{1,2\}$ indexes the spin states. As we shall see below, with the spin quantized in the $x-y$ plane a simple change of basis will transform the nominally complex generalized eigenproblem into a real generalized eigenproblem. For convenience, as the spin-$\frac{1}{2}$ basis we choose the eigenstates of S_y, expressed in terms of the S_z states, $|\uparrow\rangle$ and $|\downarrow\rangle$ as

$$|1\rangle\equiv\frac{1}{\sqrt{2}}[|\uparrow\rangle+i|\downarrow\rangle],\quad |2\rangle\equiv\frac{1}{\sqrt{2}}[|\uparrow\rangle-i|\downarrow\rangle]. \quad (2)$$

In the planar orbital basis, then, the total state is

$$|\Psi_{\mathbf{k}_\parallel}\rangle=\sum_{L',n',\mu',\sigma'}C_{L'}^{n'\mu'\sigma'}|n'\mu'\sigma';L';\mathbf{k}_\parallel\rangle, \quad (3)$$

where the expansion coefficients $C_{L'}^{n'\mu'\sigma'}$ are determined by solving the Schrödinger equation. Finally, we write the Hamiltonian as the sum of two terms, $H=H_0+H_{\rm so}$, where $H_{\rm so}$ is the spin-orbit interaction and $H_0=\mathbf{p}^2/2m+V(\mathbf{r})$, with $V(\mathbf{r})=V(\mathbf{r}+\mathbf{R}_\parallel)$ for some direct lattice vector $\mathbf{R}_\parallel$.

In the second-near-neighbor sp^3s^* model, the notation is simplified by employing 10×10 matrices $\underline{H}_{(L',L)}^{(\mu',\mu)}$ defined as (see the Appendix for explicit listings)

$$[\underline{H}_{(L',L)}^{(\mu',\mu)}]_{(n'\sigma',n\sigma)}\equiv\langle n'\mu'\sigma';L';\mathbf{k}_\parallel|H|n\mu\sigma;L;\mathbf{k}_\parallel\rangle \quad (4)$$

and ten-element vectors $\mathbf{C}_L^\mu$ defined as

$$\mathbf{C}_L^\mu\equiv[C_L^{s\mu1},C_L^{x\mu1},C_L^{y\mu1},C_L^{z\mu1},C_L^{s^*\mu1},C_L^{s\mu2},C_L^{x\mu2},C_L^{y\mu2},C_L^{z\mu2},C_L^{s^*\mu2}]^T, \quad (5)$$

where in (5) the superscript T denotes the transpose. Using this notation, the Schrödinger equation $[H-1E]|\Psi_{\mathbf{k}_\parallel}\rangle=0$ appears as pairs of equations of the form

$$[\underline{H}_{(L-1,L)}^{(a,a)}]^\dagger\mathbf{C}_{L-1}^a+[\underline{H}_{(L-1,L)}^{(c,a)}]^\dagger\mathbf{C}_{L-1}^c+[\underline{H}_{(L,L)}^{(a,a)}-\underline{1}E]\mathbf{C}_L^a+\underline{H}_{(L,L)}^{(a,c)}\mathbf{C}_L^c+\underline{H}_{(L,L+1)}^{(a,a)}\mathbf{C}_{L+1}^a=0, \quad (6)$$

$$[\underline{H}_{(L-1,L)}^{(c,c)}]^\dagger\mathbf{C}_{L-1}^c+[\underline{H}_{(L,L)}^{(a,c)}]^\dagger\mathbf{C}_L^a+[\underline{H}_{(L,L)}^{(c,c)}-\underline{1}E]\mathbf{C}_L^c+\underline{H}_{(L,L+1)}^{(c,a)}\mathbf{C}_{L+1}^a+\underline{H}_{(L,L+1)}^{(c,c)}\mathbf{C}_{L+1}^c=0. \quad (7)$$

In bulk, $\underline{H}_{(L-1,L)}^{(\mu',\mu)}=\underline{H}_{(L,L+1)}^{(\mu',\mu)}$, $(\mu',\mu)\in\{(a,a),(c,c),(c,a)\}$ and we find the complex band structure by solving either the forward, $\mathbf{C}_{L+1}^\mu=\lambda_+\mathbf{C}_L^\mu$, or reverse, $\mathbf{C}_L^\mu=\lambda_-\mathbf{C}_{L+1}^\mu$, eigenproblems; for $\lambda_\pm\neq0$, we obviously have $\lambda_-=1/\lambda_+$. Equations (6) and (7) thus constitute a 20×20, second-order eigensystem, which, however, is readily converted into a 40×40 first-order eigensystem by introducing either $\mathbf{C}_L^\mu=\lambda_+\mathbf{C}_{L-1}^\mu$ or $\mathbf{C}_{L-1}^\mu=\lambda_-\mathbf{C}_L^\mu$:

$$\lambda_+\begin{bmatrix}\underline{H}_{(L,L+1)} & \underline{0}\\ \underline{0} & \underline{1}\end{bmatrix}\begin{bmatrix}\mathbf{C}_L\\ \mathbf{C}_{L-1}\end{bmatrix}=\begin{bmatrix}-\underline{H}_{(L,L)} & -\underline{H}_{(L,L+1)}^\dagger\\ \underline{1} & \underline{0}\end{bmatrix}\times\begin{bmatrix}\mathbf{C}_L\\ \mathbf{C}_{L-1}\end{bmatrix}, \quad (8)$$

$$\begin{bmatrix}\underline{H}_{(L,L+1)} & \underline{0}\\ \underline{0} & \underline{1}\end{bmatrix}\begin{bmatrix}\mathbf{C}_L\\ \mathbf{C}_{L-1}\end{bmatrix}=\lambda_-\begin{bmatrix}-\underline{H}_{(L,L)} & -\underline{H}_{(L,L+1)}^\dagger\\ \underline{1} & \underline{0}\end{bmatrix}\times\begin{bmatrix}\mathbf{C}_L\\ \mathbf{C}_{L-1}\end{bmatrix}, \quad (9)$$

where

$$\underline{H}_{(L,L+1)}\equiv\begin{bmatrix}\underline{H}_{(L,L+1)}^{(c,c)} & \underline{H}_{(L,L+1)}^{(c,a)}\\ \underline{0} & \underline{H}_{(L,L+1)}^{(a,a)}\end{bmatrix},$$

$$\underline{H}_{(L,L)}\equiv\begin{bmatrix}[\underline{H}_{(L,L)}^{(c,c)}-\underline{1}E] & [\underline{H}_{(L,L)}^{(a,c)}]^\dagger\\ \underline{H}_{(L,L)}^{(a,c)} & [\underline{H}_{(L,L)}^{(a,a)}-\underline{1}E]\end{bmatrix}, \quad (10)$$

$$\mathbf{C}_L\equiv\begin{bmatrix}\mathbf{C}_L^c\\ \mathbf{C}_L^a\end{bmatrix}. \quad (11)$$

Note in particular from (4) and the Appendix that the matrix $\underline{H}_{(L,L)}$ is Hermitian.

The usual approach involves left-multiplying both matrices in (8) by the inverse of the matrix on the left-hand side to generate a transfer matrix, which is then diagonalized to yield eigenvalues λ_+;[2,3,11] these eigenvalues are typically written in the form $\exp[ik_za/2]$, since $a/2$ is the monolayer spacing. Those with real k_z represent propagating (Bloch) states while those with imaginary or complex k_z represent growing or decaying surface states. The difficulty with this method arises when the matrices in (8) and (9) are singular (or near-singular, as the inversions and diagonalizations are typically performed numerically), as can happen for certain $\mathbf{k}_\parallel$ or parameter sets. Now consider the case of singular matrices in (8) and (9) for some $\mathbf{k}_\parallel$. *Nothing* in the physics of the problem indicates that the complex bands should not be obtainable in these situations; certainly the bulk Hamiltonian is readily diagonalizable, yielding the real bands. This observation is further reinforced when we realize that the second-near-neighbor sp^3s^* model *can* correctly fit *both* X-valley masses; it does not exhibit the pathological, flat, transverse bands of the nearest-neighbor sp^3s^* model at the X points.

The inadequacy, therefore, lies entirely in our approach to the problem. In Sec. II C below we discuss the practical implementation of the eigenproblem, after first discussing some important properties of (8) and (9).

B. Properties of the eigensolutions

Because we introduce a method for determining the complex band structure, we must first demonstrate that the eigenvalues one finds with this method have all of the required properties. Furthermore, since we are particularly concerned with the case of singular coupling matrices, we must demonstrate these properties *without* inverting any of the matrices in question. It is not sufficient to simply *assume* these properties, especially when previous proofs of many of them (such as those given in conjunction with the transfer-matrix method[2]) involve exactly the matrix inversions we must avoid. The resulting development is therefore quite general, if slightly cumbersome.

Examining the matrices $\underline{H}_{(L',L)}^{(\mu',\mu)}$ given in the Appendix, we see that the matrices $\underline{S}_1^{\dagger}\underline{H}_{(L',L)}^{(\mu',\mu)}\underline{S}_1$ are real, where the unitary matrix $\underline{S}_1$ is defined by

$$\underline{S}_1 \equiv \begin{bmatrix} \underline{\Sigma} & \underline{0} \\ \underline{0} & \underline{\Sigma}^{\dagger} \end{bmatrix}, \quad \underline{\Sigma} \equiv \mathrm{diag}[e^{-i\pi/4}, e^{i\pi/4}, e^{i\pi/4}, e^{-i\pi/4}, e^{-i\pi/4}], \tag{12}$$

where $\mathrm{diag}[d_1, d_2, \ldots, d_n]$ denotes an $n \times n$ diagonal matrix with given (diagonal) elements. (The transformation $\underline{\Sigma}$ renders the 5×5 blocks of the nearest-neighbor, no-spin-orbit sp^3s^* Hamiltonian real.[12]) Defining a 20×20 matrix $\underline{S}_2$,

$$\underline{S}_2 \equiv \begin{bmatrix} \underline{S}_1 & \underline{0} \\ \underline{0} & \underline{S}_1 \end{bmatrix}, \tag{13}$$

then the matrices

$$\begin{bmatrix} \underline{S}_2^{\dagger} & \underline{0} \\ \underline{0} & \underline{S}_2^{\dagger} \end{bmatrix} \begin{bmatrix} \underline{H}_{(L,L+1)} & \underline{0} \\ \underline{0} & \underline{1} \end{bmatrix} \begin{bmatrix} \underline{S}_2 & \underline{0} \\ \underline{0} & \underline{S}_2 \end{bmatrix}$$

and

$$\begin{bmatrix} \underline{S}_2^{\dagger} & \underline{0} \\ \underline{0} & \underline{S}_2^{\dagger} \end{bmatrix} \begin{bmatrix} -\underline{H}_{(L,L)} & -\underline{H}_{(L,L+1)}^{\dagger} \\ \underline{1} & \underline{0} \end{bmatrix} \begin{bmatrix} \underline{S}_2 & \underline{0} \\ \underline{0} & \underline{S}_2 \end{bmatrix} \tag{14}$$

are likewise real. Since the resulting generalized eigenproblems now involve only real matrices, it follows that either (i) the eigenvalues $\lambda_{\pm}$ are real, or (ii) they come in complex-conjugate pairs: $(\lambda_{\pm}, \lambda_{\pm}^*)$. Note that this transformation *does not* double the dimension of the eigenproblem.

Another important property of (8) and (9) involves the relationship between the spectra $\{\lambda_+\}$ and $\{\lambda_-\}$. The forward eigenproblem (8) has nontrivial solutions, provided that

$$\det\begin{bmatrix} \lambda_+\underline{H}_{(L,L+1)} + \underline{H}_{(L,L)} & \underline{H}_{(L,L+1)}^{\dagger} \\ -\underline{1} & \lambda_+\underline{1} \end{bmatrix} = 0. \tag{15}$$

This determinant is easily written using the Schur complement[13] of the lower-left-hand block, $-\underline{1}$:

$$\det\begin{bmatrix} \lambda_+\underline{H}_{(L,L+1)} + \underline{H}_{(L,L)} & \underline{H}_{(L,L+1)}^{\dagger} \\ -\underline{1} & \lambda_+\underline{1} \end{bmatrix} = \det[\underline{H}_{(L,L+1)}^{\dagger} + \lambda_+\underline{H}_{(L,L)} + \lambda_+^2\underline{H}_{(L,L+1)}] = 0. \tag{16}$$

In addition, for an arbitrary matrix $\underline{A}$, $\det(\underline{A}^{\dagger}) = (\det(\underline{A}))^*$, so (16) implies

$$\det[\underline{H}_{(L,L+1)} + \lambda_+^*\underline{H}_{(L,L)} + (\lambda_+^*)^2\underline{H}_{(L,L+1)}^{\dagger}] = 0. \tag{17}$$

Examining the reverse eigenproblem (9), we see that it has nontrivial solutions provided that

$$\det\begin{bmatrix} \underline{H}_{(L,L+1)} + \lambda_-\underline{H}_{(L,L)} & \lambda_-\underline{H}_{(L,L+1)}^{\dagger} \\ -\lambda_-\underline{1} & \underline{1} \end{bmatrix} = 0, \tag{18}$$

which, expressed using the Schur complement[13] of the lower-right-hand block, $\underline{1}$, is

$$\det\begin{bmatrix} \underline{H}_{(L,L+1)} + \lambda_-\underline{H}_{(L,L)} & \lambda_-\underline{H}_{(L,L+1)}^{\dagger} \\ -\lambda_-\underline{1} & \underline{1} \end{bmatrix} = \det[\underline{H}_{(L,L+1)} + \lambda_-\underline{H}_{(L,L)} + \lambda_-^2\underline{H}_{(L,L+1)}^{\dagger}] = 0, \tag{19}$$

Comparing (17) and (19) we see that λ_+^* and λ_- satisfy the *same* polynomial equation. Now since we have already seen that for $\lambda_{\pm} \neq 0$ and $\lambda_- = 1/\lambda_+$, (17) and (19) imply that eigenvalues $\lambda_{\pm} \neq 0$ come in pairs $(\lambda_{\pm}, 1/\lambda_{\pm}^*)$. Moreover, these equations show that if $\lambda_+ = 0$ is a root of multiplicity m of (8), $\lambda_- = 0$ is likewise a root of multiplicity m of (9). Hence, even in the case of singular matrices, there are equal numbers of states which in the forward direction decay infinitely quickly ($\lambda_+ = 0$) and grow infinitely quickly ($\lambda_- = 0$).

The case of singular matrices in (8) and (9) deserves further attention. In particular, we intuitively expect that the characteristic polynomials (16) and (19) will not be of full degree (40 for the second-near-neighbor sp^3s^* model) in λ_+ and λ_-, respectively. Suppose now that $\lambda_- = 0$ is a root of multiplicity m of (19); from the foregoing discussion of (17) and (19), we know that the characteristic polynomials of the forward and reverse eigenproblems, (16) and (19) take the forms

$$\det[\underline{H}_{(L,L+1)}^{\dagger} + \lambda_+\underline{H}_{(L,L)} + \lambda_+^2\underline{H}_{(L,L+1)}] = \lambda_+^m p_+(\lambda_+) = 0, \tag{20}$$

$$\det[\underline{H}_{(L,L+1)} + \lambda_-\underline{H}_{(L,L)} + \lambda_-^2\underline{H}_{(L,L+1)}^{\dagger}] = \lambda_-^m p_-(\lambda_-) = 0, \tag{21}$$

where $\lambda_{\pm} = 0$ is *not* a root of the polynomial $p_{\pm}(\lambda_{\pm})$ and the degree of the polynomials $p_{\pm}(\lambda_{\pm})$ is certainly no greater than $40-m$. The degree of these polynomials is of particular importance for us, since only if it is less than $(40-m)$ can $\lambda_{\pm} = \infty$ be considered an ''eigenvalue'' of (8) or (9). We can determine the degree of $p_{\pm}(\lambda_{\pm})$ in the following manner. To simplify the notation, call the matrix on the left-hand side of (8) and (9) $\underline{M}_+$, and call that on the right $\underline{M}_-$. The generalized Schur decomposition theorem[14] guarantees that there exist unitary matrices $\underline{Q}$ and $\underline{Z}$ such that $\underline{Q}^{\dagger}\underline{M}_+\underline{Z} = \underline{T}_+$ and

$\underline{Q}^{\dagger}\underline{M}_{-}\underline{Z}=\underline{T}_{-}$ are upper triangular. Then, due to the unitarity of $\underline{Q}$ and $\underline{Z}$, for the forward and reverse eigenproblems we have

$$\det[\underline{M}_{-}-\lambda_{+}\underline{M}_{+}]=0\Rightarrow\det[\underline{T}_{-}-\lambda_{+}\underline{T}_{+}]=\prod_{k=1}^{40}([\underline{T}_{-}]_{k,k}-\lambda_{+}[\underline{T}_{+}]_{k,k})=0, \tag{22}$$

$$\det[\underline{M}_{+}-\lambda_{-}\underline{M}_{-}]=0\Rightarrow\det[\underline{T}_{+}-\lambda_{-}\underline{T}_{-}]=\prod_{k=1}^{40}([\underline{T}_{+}]_{k,k}-\lambda_{-}[\underline{T}_{-}]_{k,k})=0. \tag{23}$$

Equations (22) and (23) then demonstrate that m each of the diagonal elements $[\underline{T}_{-}]_{k,k}$ and $[\underline{T}_{+}]_{k,k}$ are zero. Provided that there are no corresponding zero diagonal elements, i.e., $[\underline{T}_{\mp}]_{k,k}=0\Rightarrow[T_{\pm}]_{k,k}\neq 0$, the degree of $p_{\pm}(\lambda_{\pm})$ is $(40-2m)$, *not* $(40-m)$.

Fortunately, it easy to see with the aid of this counterexample that coincident zero diagonal elements usually do not occur (we do not consider the case of trivial parameter sets). Suppose now that there is at least one pair of corresponding zero elements, say the jth, $[\underline{T}_{-}]_{j,j}=[\underline{T}_{+}]_{j,j}=0$. Obviously, in this instance, *any* complex number $\lambda_{\pm}$ is a root of (22) and (23), since the determinants are zero regardless of $\lambda_{\pm}$. Indeed, the generalized Schur decomposition theorem[14] guarantees it. If, on the other hand, we can find *some* finite $\lambda_{\pm}$ such that $\det[\underline{M}_{\mp}-\lambda_{\pm}\underline{M}_{\pm}]\neq 0$, it follows that there are *no* coincident zero-diagonal elements of the upper triangular matrices $\underline{T}_{\pm}$. Examining the blocks listed in the Appendix, we see that this is typically true, even at points such as $\mathbf{k}_{\parallel}=2\pi/a\,\mathbf{e}_x$.

We comment further that $p_{\pm}(\lambda_{\pm})$ being of degree $(40-2m)$ as opposed to $(40-m)$, is quite reasonable: the forward eigenproblem, being a polynomial equation in λ_{+} with finite coefficients, can tell us nothing about those states which grow infinitely quickly (and are in the kernel of $\underline{M}_{+}$), while the reverse eigenproblem can likewise tell us nothing of the states in the kernel of $\underline{M}_{-}$. Assuming that the geometric and algebraic multiplicities of all eigenvalues coincide (even for $\lambda_{\pm}=0$), we have a 40-state basis by taking the m states in $\ker(\underline{M}_{+})$, the m states in $\ker(\underline{M}_{-})$, and the $(40-2m)$ states for which $\lambda_{\pm}\neq 0$ (so that $\lambda_{-}=1/\lambda_{+}$), half of which decay or propagate forward, and half of which decay or propagate backward, the last assertion being guaranteed by the properties of the $\lambda_{\pm}$ derived above. (The assumption that these states form a basis is also made when the states come from diagonalizing a transfer matrix.) This discussion furthermore demonstrates the difficulties of a method (such as that of Chang[6]) which seeks the roots of only *one* of the equations (20) and (21): in the singular case here considered only $(40-m)$ roots can be found. It is therefore imperative to be careful in the implementation of such a model for singular and near-singular cases. We shall use the foregoing analysis as a guide in selecting an implementation scheme.

C. Practical implementation

On first inspection it appears necessary to solve both the forward and reverse eigenproblems, (8) and (9), owing to the possibility of infinite ''eigenvalues,'' which occur when $\underline{M}_{+}$ and $\underline{M}_{-}$ are singular. Fortunately, it turns out that all eigenvalues $\lambda_{\pm}$ and corresponding eigenvectors may be determined in a single diagonalization using EISPACK routines to solve a real, generalized, eigensystem.[15] Because the EISPACK routines are written for real matrices, we first apply the straightforward transformation discussed at the beginning of Sec. II B above to make the problem real; we previously used this transformation to show that complex eigenvalues $\lambda_{\pm}$ come in complex-conjugate pairs: $(\lambda_{\pm},\lambda_{\pm}^{*})$. A single diagonalization step suffices since, for the real generalized eigensystem $\underline{A}\mathbf{x}=\lambda\underline{B}\mathbf{x}$, the EISPACK routines determine pairs of scalars α and β such that

$$\beta\underline{A}\mathbf{x}=\alpha\underline{B}\mathbf{x}, \tag{24}$$

where, for $\beta\neq 0$, $\lambda=\alpha/\beta$. Eigenvectors $\mathbf{x}$ corresponding to infinite ''eigenvalues'' thus have $|\beta|\approx 0$, while those with $\mathbf{x}$ corresponding to $\lambda=0$ have $|\alpha|\approx 0$. Hence in a single calculation we determine not only the eigenvectors $\mathbf{x}$, for which $\alpha,\beta\neq 0$, but as well those $\mathbf{x}$ lying in $\ker(\underline{A})$ (i.e., $|\alpha|\approx 0$) and in $\ker(\underline{B})$ (i.e., $|\beta|\approx 0$).

TABLE II. Energy gaps and effective masses reproduced by the tight-binding parameters of Table I; m_0 is the free-electron mass.

Quantity	GaAs	AlAs	Units
$E_g(\Gamma)$	1.398	2.998	eV
$E_g(X)$	1.803	2.142	eV
$E_g(L)$	1.642	2.313	eV
Δ_0	0.369	0.337	eV
m_{Γ}^{*}	0.067	0.18	m_0
$m_{X,l}^{*}$	1.42	1.44	m_0
$m_{X,t}^{*}$	0.31	0.25	m_0
$m_{L,l}^{*}$	1.43	1.18	m_0
$m_{L,t}^{*}$	0.13	0.16	m_0
m_{lh}^{*}	0.069	0.15	m_0
m_{hh}^{*}	0.39	0.43	m_0
m_{so}^{*}	0.14	0.24	m_0

III. RESULTS AND DISCUSSION

The tight-binding parameters for the second-nearest-neighbor sp^3s^* Hamiltonian, including spin-orbit interactions, are listed in Table I; note that we *do not* make the two-center approximation. Table II gives the effective masses and band gaps they reproduce, and the band structures are shown in Figs. 1 and 2. The parameters have been chosen to fit the gaps at $T=300$ K. In general, we find it possible to closely fit the direct and indirect gaps, as well as the Γ- and X-valley masses, although the X-valley transverse masses are about 25% too large. The L-valley effective masses are not as well reproduced—the longitudinal masses are too small and the transverse masses are too large; they are, however, not unreasonable in view of the number of

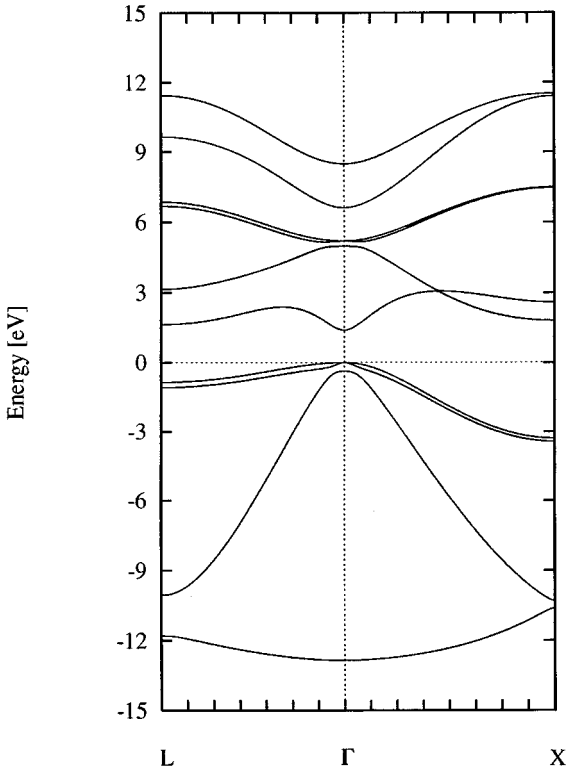

FIG. 1. Real bands of GaAs as reproduced by the parameters of Table I.

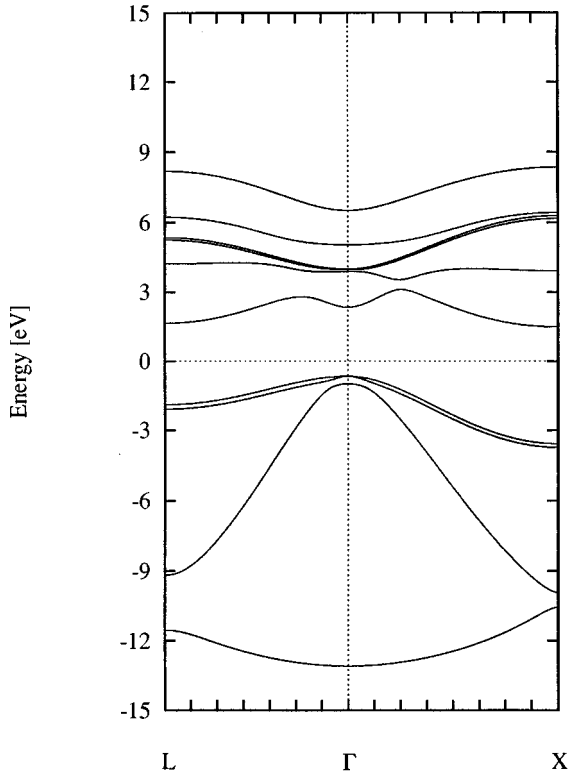

FIG. 2. Real bands of AlAs as reproduced by the parameters of Table I.

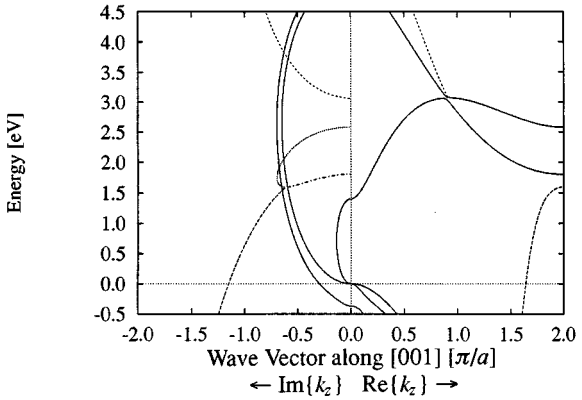

FIG. 3. Complex bands of GaAs as reproduced by the parameters of Table I. Solid lines represent purely real or imaginary bands, while pairs of broken lines graph the real and imaginary parts of complex bands; real bands and parts appear in the right panel, imaginary bands and parts in the left. Real parts which appear to be missing actually lie at the zone boundary, and thus are obscured by the border. To enhance readability we omit highly evanescent complex and imaginary bands (those with large Im$\{k_z\}$).

quantities we attempted to fit. In the valence bands, we concentrated on fitting the light-hole mass, since the imaginary band linking the light-hole valence-band maximum to the conduction-band minimum at Γ is important in tunneling calculations. Overall, the fit of the bands, particularly the conduction band, is superior to that achieved by Talwar and Ting[4] using the second-near-neighbor sp^3 model; with the addition of the excited s-like s^* orbital, it has become possible to achieve the deep curvature necessary to fit the GaAs Γ-valley conduction-band mass.

The complex bands for the [001] face of GaAs and AlAs are shown in Figs. 3 and 4, respectively. In the figures solid lines represent purely real or imaginary bands, while pairs of broken lines graph the real and imaginary parts of complex

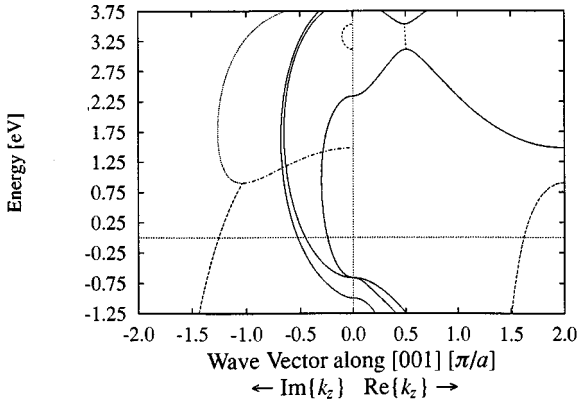

FIG. 4. Complex bands of AlAs as reproduced by the parameters of Table I. Solid lines represent purely real or imaginary bands, while pairs of broken lines graph the real and imaginary parts of complex bands; real bands and parts appear in the right panel, imaginary bands and parts in the left. Real parts which appear to be missing actually lie at the zone boundary, and thus are obscured by the border. To enhance readability we omit highly evanescent complex and imaginary bands (those with large Im$\{k_z\}$).

bands; real bands and parts appear in the right panels, imaginary bands and parts in the left. To enhance readability we omit from both figures highly evanescent complex and imaginary bands (those with large $\mathrm{Im}\{k_z\}$). The complex bands were calculated with the method of Sec. II above. The value of this method is further underscored by using it to evaluate the effective mass of the conduction band numerically for a value of $\mathbf{k}_\parallel$, say, $\mathbf{k}_\parallel=2\pi/a\mathbf{e}_x$, at which a transfer matrix does not exist. Consider the X-valley transverse mass at this point. The value listed in Table II is computed from the bulk Hamiltonian, $H(\mathbf{k})$, and its derivatives, $\nabla_{\mathbf{k}}H(\mathbf{k})$, and $\partial^2 H(\mathbf{k})/\partial k^{(\alpha)}\partial k^{(\beta)}$, using the eigenvectors of $H(\mathbf{k})$ at $\mathbf{k}=2\pi/a\mathbf{e}_x$.[16] On the other hand, we may also choose closely spaced values of E for $\mathbf{k}_\parallel=2\pi/a\mathbf{e}_x$, solve the forward eigenproblem (8), and select the eigenvalues $\exp[ik_z a/2]$ corresponding to the X valley (thus yielding three closely spaced, z wave vectors, $k_z\in\mathrm{Re}$). Doing so and fitting the resulting three points to a parabola, we find $m^*_{X,t}\approx 0.31 m_0$ for GaAs, in excellent agreement with the other calculation.

IV. SUMMARY AND CONCLUSIONS

In conclusion, we have presented a method for calculating surface and interface states; that is, the eigenvalues (propagation factors) and eigenvectors of a bulk crystal in the planar-orbital basis. This method is applicable even in those situations in which a transfer matrix does not exist (for example, at certain values of the in-plane wave vector $\mathbf{k}_\parallel$). We have also provided parametrizations for GaAs and AlAs in the second-near-neighbor sp^3s^* model, achieving a superior fit of the conduction bands to that afforded by the either the nearest-neighbor sp^3s^* or second-near-neighbor sp^3 models. We have applied the method to the first of these models and analyzed it, showing that even in cases in which a transfer matrix does not exist the complex bands still have all the required properties. In addition, we have provided transformations necessary to turn the nominally complex problem into a real one, thus allowing a more efficient implementation. Furthermore, we have shown how and why this method succeeds in those situations where previous methods for calculating the complex band structure fail. The generality of this method, together with the superior fit achieved in the second-near-neighbor sp^3s^* model, makes their combination a good choice for the underlying tight-binding model in tunneling calculations involving indirect semiconductors and/or inelastic processes.

ACKNOWLEDGMENTS

We thank R. C. Bowen, D. Jovanovic, G. Klimeck, and R. Lake for stimulating discussions and comments, and we gratefully acknowledge Texas Instruments, Inc. for supporting this work.

APPENDIX

Here we present the blocks of the second-near-neighbor sp^3s^* Hamiltonian in the planar-orbital basis. The 10×10 blocks appearing in (6), (7), and (10) are the intralayer coupling matrices

$$\underline{H}^{(\mu,\mu)}_{(L,L)}=\begin{bmatrix}\underline{H}^{(\mu,\mu)}_{0(L,L)}+\underline{h}^{(\mu)}_{\mathrm{so}}(1,1) & \underline{h}^{(\mu)}_{\mathrm{so}}(1,2)\\ \underline{h}^{(\mu)\dagger}_{\mathrm{so}}(1,2) & \underline{H}^{(\mu,\mu)}_{0(L,L)}+\underline{h}^{(\mu)*}_{\mathrm{so}}(1,1)\end{bmatrix}, \tag{A1}$$

and the interlayer and intersublayer coupling matrices

$$\underline{H}^{(\mu,\mu')}_{(\Lambda,\Lambda')}=\begin{bmatrix}\underline{H}^{(\mu,\mu)}_{0(\Lambda,\Lambda')} & \underline{0}\\ \underline{0} & \underline{H}^{(\mu,\mu)}_{0(\Lambda,\Lambda')}\end{bmatrix} \tag{A2}$$

where in (A1), $\mu=a$ or c and in (A2) $\{(\mu,\mu'),(\Lambda,\Lambda')\}=\{(a,a),(L,L+1)\}$, $\{(c,c),(L,L+1)\}$, $\{(a,c),(L,L)\}$, or $\{(c,a),(L,L+1)\}$.

Below we list the explicit forms of the 5×5 matrices appearing in (A1) and (A2); as above, $\mu=a$ or c. To enhance readability we introduce the following notations for nearest-neighbor geometric factors and parameters:

$$c_\pm\equiv\cos[(k_x\pm k_y)a/4],\quad s_\pm\equiv\sin[(k_x\pm k_y)a/4], \tag{A3}$$

$$v(\alpha\mu,\beta\nu)\equiv 2E^{(\frac{1}{2}\frac{1}{2}\frac{1}{2})}_{\alpha\mu,\beta\nu}, \tag{A4}$$

and for second-near-neighbor geometric factors and parameters,

$$C_\nu\equiv\cos(k_\nu a/2),\quad S_\nu\equiv\sin(k_\nu a/2),\quad \nu\in\{x,y\}, \tag{A5}$$

$$\widetilde{E}^{(011)}_{\alpha\mu,\beta\mu}\equiv\begin{cases}E^{(011)}_{\alpha a,\beta a}, & \mu=a\\ -E^{(011)}_{\alpha c,\beta c}, & \mu=c,\end{cases} \tag{A6}$$

where $(\alpha,\beta)\in\{(s,x),(s^*,x),(x,y)\}$.

The 5×5 matrices appearing in (A1) appear below. Note that the spin-orbit matrices appear different due to our use of the eigenstates of S_y for the spin-$\frac{1}{2}$ basis states:

$$\underline{h}^{(\mu)}_{\mathrm{so}}(1,1)=\begin{bmatrix}0&0&0&0&0\\0&0&0&i\lambda_\mu&0\\0&0&0&0&0\\0&-i\lambda_\mu&0&0&0\\0&0&0&0&0\end{bmatrix}, \tag{A7}$$

$$\underline{h}^{(\mu)}_{\mathrm{so}}(1,2)=\begin{bmatrix}0&0&0&0&0\\0&0&-i\lambda_\mu&0&0\\0&i\lambda_\mu&0&-\lambda_\mu&0\\0&0&\lambda_\mu&0&0\\0&0&0&0&0\end{bmatrix}. \tag{A8}$$

The other matrices are

$$\underline{\underline{H}}^{(\mu,\mu)}_{0(L,L)}=\begin{bmatrix} E^{(000)}_{s\mu,s\mu} & 0 & 0 & 0 & 0 \\ 0 & E^{(000)}_{x\mu,x\mu} & 0 & 0 & 0 \\ 0 & 0 & E^{(000)}_{x\mu,x\mu} & 0 & 0 \\ 0 & 0 & 0 & E^{(000)}_{x\mu,x\mu} & 0 \\ 0 & 0 & 0 & 0 & E^{(000)}_{s*\mu,s*\mu} \end{bmatrix}+\begin{bmatrix} 4E^{(110)}_{s\mu,s\mu}C_xC_y & i4E^{(110)}_{s\mu,x\mu}S_xC_y & i4E^{(110)}_{s\mu,x\mu}C_xS_y & -4\widetilde{E}^{(011)}_{s\mu,x\mu}S_xS_y & 4E^{(110)}_{s\mu,s*\mu}C_xC_y \\ -i4E^{(110)}_{s\mu,x\mu}S_xC_y & 4E^{(110)}_{x\mu,x\mu}C_xC_y & -4E^{(110)}_{x\mu,y\mu}S_xS_y & -i4\widetilde{E}^{(011)}_{x\mu,y\mu}C_xS_y & -i4E^{(110)}_{s*\mu,x\mu}S_xC_y \\ -i4E^{(110)}_{s\mu,x\mu}C_xS_y & -4E^{(110)}_{x\mu,y\mu}S_xS_y & 4E^{(110)}_{x\mu,x\mu}C_xC_y & -i4\widetilde{E}^{(011)}_{x\mu,y\mu}S_xC_y & -i4E^{(110)}_{s*\mu,x\mu}C_xS_y \\ -4\widetilde{E}^{(011)}_{s\mu,x\mu}S_xS_y & i4\widetilde{E}^{(011)}_{x\mu,y\mu}C_xS_y & i4\widetilde{E}^{(011)}_{x\mu,y\mu}S_xC_y & 4E^{(011)}_{x\mu,x\mu}C_xC_y & -4\widetilde{E}^{(011)}_{s*\mu,x\mu}S_xS_y \\ 4E^{(110)}_{s\mu,s*\mu}C_xC_y & i4E^{(110)}_{s*\mu,x\mu}S_xC_y & i4E^{(110)}_{s*\mu,x\mu}C_xS_y & -4\widetilde{E}^{(011)}_{s*\mu,x\mu}S_xS_y & 4E^{(110)}_{s*\mu,s*\mu}C_xC_y \end{bmatrix}. \tag{A9}$$

The interlayer and intersublayer coupling matrices appearing in (A2) are

$$\underline{\underline{H}}^{(\mu,\mu)}_{0(L,L+1)}=\begin{bmatrix} 2E^{(110)}_{s\mu,s\mu}(C_x+C_y) & i2(E^{(110)}_{s\mu,x\mu}S_x+\widetilde{E}^{(011)}_{s\mu,x\mu}S_y) & i2(E^{(110)}_{s\mu,x\mu}S_y+\widetilde{E}^{(011)}_{s\mu,x\mu}S_x) & 2E^{(110)}_{s\mu,x\mu}(C_x+C_y) & 2E^{(110)}_{s\mu,s*\mu}(C_x+C_y) \\ i2(\widetilde{E}^{(011)}_{s\mu,x\mu}S_y-E^{(110)}_{s\mu,x\mu}S_x) & 2(E^{(110)}_{x\mu,x\mu}C_x+E^{(011)}_{x\mu,x\mu}C_y) & 2\widetilde{E}^{(011)}_{x\mu,y\mu}(C_y-C_x) & i2(E^{(110)}_{x\mu,y\mu}S_x+\widetilde{E}^{(011)}_{x\mu,y\mu}S_y) & i2(\widetilde{E}^{(011)}_{s*\mu,x\mu}S_y-E^{(110)}_{s*\mu,x\mu}S_x) \\ i2(\widetilde{E}^{(011)}_{s\mu,x\mu}S_x-E^{(110)}_{s\mu,x\mu}S_y) & 2\widetilde{E}^{(011)}_{x\mu,y\mu}(C_x-C_y) & 2(E^{(011)}_{x\mu,x\mu}C_x+E^{(110)}_{x\mu,x\mu}C_y) & i2(E^{(110)}_{x\mu,y\mu}S_y+\widetilde{E}^{(011)}_{x\mu,y\mu}S_x) & i2(\widetilde{E}^{(011)}_{s*\mu,x\mu}S_x-E^{(110)}_{s*\mu,x\mu}S_y) \\ -2E^{(110)}_{s\mu,x\mu}(C_x+C_y) & i2(E^{(110)}_{x\mu,y\mu}S_x-\widetilde{E}^{(011)}_{x\mu,y\mu}S_y) & i2(E^{(110)}_{x\mu,y\mu}S_y-\widetilde{E}^{(011)}_{x\mu,y\mu}S_x) & 2E^{(110)}_{x\mu,x\mu}(C_x+C_y) & -2E^{(110)}_{s*\mu,x\mu}(C_x+C_y) \\ 2E^{(110)}_{s\mu,s*\mu}(C_x+C_y) & i2(E^{(110)}_{s*\mu,x\mu}S_x+\widetilde{E}^{(011)}_{s*\mu,x\mu}S_y) & i2(E^{(110)}_{s*\mu,x\mu}S_y+\widetilde{E}^{(011)}_{s*\mu,x\mu}S_x) & 2E^{(110)}_{s*\mu,x\mu}(C_x+C_y) & 2E^{(110)}_{s*\mu,s*\mu}(C_x+C_y) \end{bmatrix}, \tag{A10}$$

$$\underline{\underline{H}}^{(a,c)}_{0(L,L)}=\begin{bmatrix} \nu(sa,sc)c_+ & i\nu(sa,pc)s_+ & i\nu(sa,pc)s_+ & \nu(sa,pc)c_+ & \nu(sa,s*c)c_+ \\ -i\nu(pa,sc)s_+ & \nu(x,x)c_+ & \nu(x,y)c_+ & i\nu(x,y)s_+ & -i\nu(pa,s*c)s_+ \\ -i\nu(pa,sc)s_+ & \nu(x,y)c_+ & \nu(x,x)c_+ & i\nu(x,y)s_+ & -i\nu(pa,s*c)s_+ \\ -\nu(pa,sc)c_+ & i\nu(x,y)s_+ & i\nu(x,y)s_+ & \nu(x,x)c_+ & -\nu(pa,s*c)c_+ \\ v(s*a,sc)c_+ & i\nu(s*a,pc)s_+ & i\nu(s*a,pc)s_+ & \nu(s*a,pc)c_+ & \nu(s*a,s*c)c_+ \end{bmatrix}, \tag{A11}$$

$$\underline{\underline{H}}^{(c,a)}_{0(L,L+1)}=\begin{bmatrix} v(sa,sc)c_- & i\nu(pa,sc)s_- & -i\nu(pa,sc)s_- & \nu(pa,sc)c_- & \nu(s*a,sc)c_- \\ -i\nu(sa,pc)s_- & \nu(x,x)c_- & -\nu(x,y)c_- & i\nu(x,y)s_- & -i\nu(s*a,pc)s_- \\ i\nu(sa,pc)s_- & -\nu(x,y)c_- & \nu(x,x)c_- & -i\nu(x,y)s_- & i\nu(s*a,pc)s_- \\ -\nu(sa,pc)c_- & i\nu(x,y)s_- & -i\nu(x,y)s_- & \nu(x,x)c_- & -\nu(s*a,pc)c_- \\ \nu(sa,s*c)c_- & i\nu(pa,s*c)s_- & -i\nu(pa,s*c)s_- & \nu(pa,s*c)c_- & \nu(s*a,s*c)c_- \end{bmatrix}. \tag{A12}$$

*Electronic address: boykin@amadeus.eb.uah.edu

[1] P. Vogl, Harold P. Hjalmarson, and John D. Dow, J. Phys. Chem. Solids **44**, 365 (1983).
[2] D. H. Lee and J. D. Joannopoulos, Phys. Rev. B **23**, 4988 (1981); J. Vac. Sci. Technol. **19**, 355 (1981).
[3] Timothy B. Boykin, Jan P. A. van der Wagt, and James S. Harris, Jr., Phys. Rev. B **43**, 4777 (1991).
[4] D. N. Talwar and C. S. Ting, Phys. Rev. B **25**, 2660 (1982).
[5] C. Tserbak, H. M. Polatoglu, and G. Theodorou, Phys. Rev. B **47**, 7104 (1992).
[6] Yia-Chung Chang, Phys. Rev. B **25**, 605 (1982).
[7] Yia-Chung Chang and J. N. Schulman, Phys. Rev. B **25**, 3975 (1982).
[8] R. Chris Bowen, William R. Frensley, Gerhard Klimeck, and Roger K. Lake, Phys. Rev. B **52**, 2754 (1995).
[9] J. C. Slater and G. F. Koster, Phys. Rev. **94**, 1498 (1954).
[10] K. C. Haas, H. Ehrenreich, and B. Velicky, Phys. Rev. B **27**, 1088 (1983).
[11] D. Z.-Y. Ting, E. T. Yu, and T. C. McGill, Phys. Rev. B **45**, 3583 (1992).
[12] Jan P. A. van der Wagt and Timothy B. Boykin (unpublished).
[13] Peter Lancaster and Myron Tismenetsky, *The Theory of Matrices*, 2nd ed. (Academic, Orlando, FL, 1985), p. 46.
[14] Gene H. Golub and Charles F. Van Loan, *Matrix Computations*, 2nd ed. (Johns Hopkins University Press, Baltimore, 1989), pp. 394–396.
[15] B. S. Grabow, J. M. Boyle, J. J. Dongarra, and C. B. Moler, *Matrix Eigensystem Routines: EISPACK Guide Extension* (Springer-Verlag, New York, 1977) Secs. 2.1.9, 2.1.10, 2.3.1, 2.3.2, and 7.1. In our implementation we use *C*-language translations of EISPACK routines qzhes, qzit, qzval, and qzvec.
[16] Timothy B. Boykin, Phys. Rev. B **52**, 16 317 (1995).